Indian Journal of Chemistry
Vol. 64, May 2025, pp. 476-485
DOI: 10.56042/ijc.v64i5.12581

Effect of temperature and solvents on thermo-physical properties of pyrimidine substituted thiazolidinone derivatives at three different temperatures

Umang P Mehta, Dinesh R Godhani*, Anwar H Saiyad, Kuldip P Parmar & Jignasu P Mehta

Department of Chemistry (DST-FIST sponsored Department), Mahatma Gandhi Campus, Maharaja Krishnakumarsinhji Bhavnagar University, Bhavnagar 364 002, India

E-mail:drgodhani@mkbhavuni.edu.in

Received 18 July 2024; accepted(revised) 28 April 2025

Ultrasonic velocities, densities, and viscosities have been determined in a binary liquid tandem including pyrimidine substituted thiazolidinone at temperatures T= (298.15, 308.15, and 313.15 K) over the thiazolidinone's complete molality range. 5-(4-fluorobenzylidene)-2-(furan-2-yl)-3-(pyrimidin-2-yl)thiazolidin-4-one **(AZ_1)** and 2-(furan-2-yl)-5-(4-methylbenzylidene)-3-(pyrimidin-2-yl)thiazolidin-4-one **(AZ_2)** in N,N-dimethyl formamide (DMF) and dimethylsulfoxide (DMSO) were studied. Further to various acoustical and thermodynamic parameters, measurements have been made of the density, viscosity, and ultrasonic sound velocity. Further study has been conducted to figure out the effects of solvent alterations and structural modifications on the values of Gibbs energy of activation (ΔG^*), enthalpy of activation (ΔH^*), and entropy of activation (ΔS^*). These results have been explained in terms of the molecular interactions among the constituents of the liquid mixture.

Keywords: Density, Sound velocity, Gibbs energy of activation, Acoustical parameters

Several investigations have been done involving ultrasonic sound, and there are many noteworthy potential uses for it in biology, medicine, engineering, and polymer synthesis[1-2]. Likewise, the way materials are categorized and how ultrasound is applied in method observation[3]. Information on the bulk characteristics and intermolecular forces may be provided from ultrasonic sound velocity (U), viscosity (η), and density (ρ)[4-5]. They are included in several industrial processes and goods. The biochemical sector also uses ultrasonic sound in an array of applications[6]. Ultrasonic sound waves are used in synthetic organic chemistry to forecast the occurrence of phase transition materials, increase yield, decrease reaction temperatures, and speed up processes, among other things[7]. In order to examine the nature of molecular interactions in various binary[8-9] and ternary[10] liquid mixes, sound velocity measurements have also been utilized. This method has been used by several researchers to a variety of solutions, such as polymers[11], other electrolytes[12], and non-electrolytes[13]. The furan substituted thiazolidinone molecule's antibacterial[16], anticonvulsant[15], and anticancer[14] characteristics have garnered the greatest interest in biological applications.

The current analysis defines the influence of temperature and two different solvents on the molecular interactions of 5-(4-bromobenzylidene)-2-(furan-2-yl)-3-(pyrimidin-2-yl)thiazolidin-4-one **(AZ_1)** and 2-(furan-2-yl)-5-(4-methoxybenzylidene)-3-(pyrimidin-2-yl)thiazolidin-4-one **(AZ_2)** and thereby effect on thermo-acoustical considerations at atmospheric pressure. The results are explained in terms of molecular interaction that appears in the mixture.

Experimental Section

Materials and Methods

The chemicals utilized in the current experiment are AnalaR grade and came from Spectrochem chemicals. The compounds are purified using accepted practices. The 5-(4-bromobenzylidene)-2-(furan-2-yl)-3-(pyrimidin-2-yl) thiazolidin-4-one **(AZ_1)**2-(furan-2-yl)-5-(4-methoxybenzylidene)-3-(pyrimidin-2-yl)thiazolidin-4-one **(AZ_2)** utilized in this investigation were made in our lab (Table 1). Additional information is provided in the supplemental data. Fig. 1 depicts the structures of the recently synthesized compounds **AZ_1** and **AZ_2**.(0.001-0.010 mol·kg^{-1}) in DMSO and DMF

Table 1 — Chemicals used in this work.

Chemicals	Source	Mole fraction purities (by manufacturer)	Mole fraction purities(obtained by GC)
DMSO	SpectrochemPvt.Ltd.	0.996	0.995
DMF	SpectrochemPvt.Ltd.	0.995	0.993
AZ_1	Synthesis	-	0.995
AZ_2	Synthesis	-	0.992

Table 2 — Comparison of measured density, ρ, viscosity, η, and ultrasonic velocity, U data for pure DMSO and DMF with literature values at T = (298.15, 308.15, and 318.15) K.

Organic liquids	This work			Literature		
	T = 298.15 K	T = 308.15 K	T = 318.15 K	T = 298.15 K	T = 308.15 K	T = 318.15 K
				ρ / (kg · m^{-3})ρ / (kg · m^{-3})		
DMSO	1095.34	1085.16	1075.19	1095.29 [18]	1085.25 [18]	1075.21[18]
DMF	943.95	934.39	924.78	943.94[21]	934.64 [21]	925.80 [22]
				η / (mPa·s)η / (mPa· s)		
DMSO	1.8613	1.4748	1.2581	1.8480 [18]	1.4980 [18]	1.310 [19]
DMF	0.8072	0.7064	0.6174	0.8040 [23]	0.7103 [21]	0.6348 [21]
				U / (m · s^{-1})U / (m · s^{-1})		
DMSO	1484.4	1450.8	1416.8	1485.1 [20]	1451.3 [20]	1417.7 [20]
DMF	1457.11	1418.04	1379.81	1457.49 [21]	1418.95 [21]	1379.60 [24]

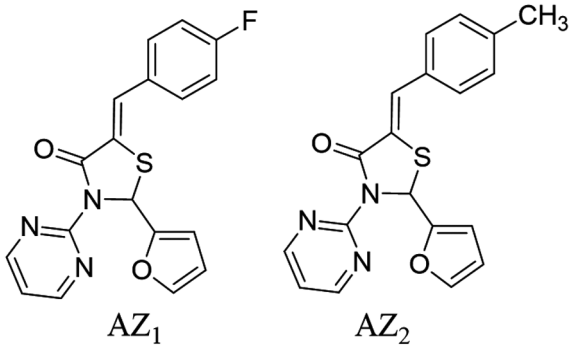

Fig. 1 — Structure of 5-(4-fluorobenzylidene)-2-(furan-2-yl)-3-(pyrimidin-2-yl)thiazolidin-4-one (AZ_1) and 2-(furan-2-yl)-5-(4-methylbenzylidene)-3-(pyrimidin-2-yl)thiazolidin-4-one (AZ_2)

were made at three different temperatures *viz*. Using the M-81 multi-frequency ultrasonic interferometer (2 MHz) (Mittal Enterprise, New Delhi), measurements of ultrasonic sound velocity, viscosity, and density in pure solvents (DMSO and DMF) and solutions of both compounds (0.001-0.010 mol·kg^{-1}) in DMSO and DMF were made at three different temperatures, namely (298.15, 308.15, and 318.15 K). With an accuracy of 0.5°C, the temperature was managed using the digital temperature controller of the Instrucare solution viscosity bath. The automatic density meter (DDM2909) from Rudolf Research Analytical was utilized to measure density. Fungilabviscolead advance viscometer was used for the viscosity measurement. Ultrasonic sound velocity(U), density (ρ) and viscosity (η) measurements were accurate to ±1%, ±0.0002 g·cm^{-3} and ±0.40%, respectively. The uncertainty of temperature is ±0.1K and that of concentration measured is ±0.001mol·dm^{-3}. To determine each sample's solubility at the requisite temperature, Sonixvibra-cell (VCX500) was used to prepare them all afresh. Each sample was then kept at the temperature for 24 h. Samples were kept in bottles with vacuum sealing until use. Numerous acoustical factors are computed using conventional equations from the experimental data of ρ, η and U [17].

Results and Discussion

When compared to the data from the available literature, the standard data of dimethyl sulfoxide (DMSO) and N, N-dimethyl formamide's (DMF) density, viscosity, and ultrasonic velocity used in the current analysis are given in Table 2. This indicates an acceptable level of coherence between theoretical and practical data. Additionally, it appeared from the findings that our testing had perfect standardization and calibration. The density (ρ), viscosity (η), and ultrasonic velocity (U) of pure solvents and AZ_1 and AZ_2 solutions in DMSO and DMF that were measured at T = (298.15, 308.15, and 318.15) K are summarized in Table 3 and Table 4. It is evident from Table 5, 6, 7, and 8 that concentration (C) and temperature (T) have the opposite effects on ultrasonic velocity (U), viscosity (η), and density (ρ).The influence of temperature and concentration on these data were examined using least squares analysis. Figs. 2, 3, 4, 5, 6, and 7 illustrate the experimentally determined correlations between density (ρ) and concentration (C) (R^2 = 0.978–0.999), viscosity (η) and concentration (C) (R^2 = 0.931-0.999), and

Table 3 — The density, ρ, viscosity, η, and ultrasonic velocity, U, for AZ_1 in DMSO and DMF solutions at T = (298.15, 308.15, and 318.15) K and at atmospheric pressure.

DMSO + AZ_1 system				DMF + AZ_1 system			
$m^a \cdot 10^{-3}$/(mol· kg^{-1})	ρ /(kg · m^{-3})	η /(mPa· s)	U /(m · s^{-1})	$m^a \cdot 10^{-3}$ /(mol· kg^{-1})	ρ /(kg · m^{-3})	η /(mPa· s)	U /(m · s^{-1})
T = 298.15 K				T = 298.15 K			
0	1095.34	1.8613	1484.4	0	943.95	0.8072	1457.1
0.91225	1096.55	1.8824	1499.5	1.05832	945.26	0.8331	1457.3
1.82417	1097.12	1.9616	1501.2	2.11500	946.36	0.8437	1458.6
3.64926	1097.58	2.0195	1503.1	4.22301	948.66	0.8644	1460.4
5.47412	1098.27	2.0728	1504.8	6.32567	950.72	0.8867	1462.1
7.29966	1098.88	2.1632	1505.6	8.42158	952.88	0.9110	1463.7
9.12695	1099.33	2.2367	1506.8	10.51032	955.12	0.9298	1465.6
T = 308.15 K				T = 308.15 K			
0	1085.16	1.4748	1450.8	0	934.39	0.7064	1418.0
0.92094	1086.21	1.5074	1462.2	1.06930	935.55	0.7203	1418.7
1.84120	1086.98	1.5384	1463.5	2.13461	937.67	0.7325	1419.6
3.68266	1087.64	1.5709	1465.1	4.26630	939.05	0.7516	1421.1
5.52295	1088.58	1.6024	1467.4	6.38450	941.98	0.7705	1422.5
7.36430	1089.26	1.6351	1468.7	8.50131	943.97	0.7864	1423.9
9.20466	1090.08	1.6684	1469.8	10.62139	945.17	0.7977	1425.5
T = 318.15 K				T = 318.15 K			
0	1075.19	1.2581	1416.8	0	924.78	0.6174	1379.8
0.92953	1076.17	1.2965	1431.7	1.07925	926.93	0.6281	1380.6
1.85850	1076.87	1.3316	1432.4	2.15916	927.02	0.6349	1381.6
3.71719	1077.55	1.3927	1433.8	4.31043	929.45	0.6466	1383.0
5.57529	1078.38	1.4089	1435.9	6.45650	931.50	0.6613	1384.9
7.43362	1079.13	1.4471	1437.5	8.59013	934.24	0.6732	1386.2
9.29181	1079.89	1.4832	1438.4	10.73104	935.55	0.6867	1387.7

[a]molality of AZ_1 in DMSO and DMF solutions at different temperatures in mol· kg^{-1}.
All the measurements were carried out at atmospheric pressure.

Table 4 — The density, ρ, viscosity, η, and ultrasonic velocity, U, forAZ_2 in DMSO and DMF solutions at T = (298.15, 308.15, and 318.15) K and at atmospheric pressure.

DMSO + AZ_2 system				DMF + AZ_2 system			
$m^a \cdot 10^{-3}$/(mol· kg^{-1})	ρ /(kg · m^{-3})	η /(mPa· s)	U /(m · s^{-1})	$m^a \cdot 10^{-3}$ /(mol· kg^{-1})	ρ /(kg · m^{-3})	η /(mPa· s)	U /(m · s^{-1})
T = 298.15 K				T = 298.15 K			
0	1095.34	1.8613	1484.4	0	943.95	0.8072	1457.1
0.91256	1096.20	1.8813	1499.6	1.04839	954.22	0.8385	1457.8
1.82491	1096.71	1.9433	1501.2	2.09403	955.86	0.8504	1458.7
3.65028	1097.34	2.0053	1503.2	4.18201	958.01	0.8711	1460.5
5.47835	1097.52	2.0673	1505.2	6.26272	960.35	0.8936	1462.1
7.30385	1098.38	2.1323	1506.4	8.33800	962.53	0.9165	1463.5
9.13170	1098.92	2.1973	1508.0	10.40749	964.68	0.9377	1465.1
T = 308.15 K				T = 308.15 K			
0	1085.16	1.4748	1450.8	0	934.39	0.7064	1418.0
0.92073	1086.47	1.4807	1462.8	1.05968	944.06	0.7236	1419.1
1.84093	1087.17	1.5092	1464.4	2.11765	945.21	0.7357	1420.0
3.68291	1087.63	1.5385	1466.4	4.23022	947.11	0.7583	1421.7
5.52476	1088.32	1.5667	1468.4	6.32704	950.61	0.7765	1423.1
7.36782	1088.87	1.5991	1469.2	8.42351	952.79	0.7954	1424.6
9.21017	1089.59	1.6334	1470.4	10.52193	954.23	0.8041	1426.4
T = 318.15 K				T = 318.15 K			
0	1075.19	1.2581	1416.8	0	924.78	0.6174	1379.8
0.92965	1076.05	1.2851	1432.0	1.07093	934.15	0.6291	1380.9
1.85883	1076.71	1.3408	1433.2	2.13909	935.74	0.6379	1382.1
3.71800	1077.38	1.3982	1434.4	4.27379	937.47	0.6506	1383.7
5.57688	1078.17	1.4079	1436.0	6.39741	940.18	0.6633	1385.4
7.43838	1078.57	1.4434	1437.2	8.51351	942.75	0.6762	1386.8
9.29803	1079.33	1.4789	1439.2	10.63517	944.11	0.6911	1388.2

[a]molality of AZ_2 in DMSO and DMF solutions at different temperatures in mol· kg^{-1}.
All the measurements were carried out at atmospheric pressure.

Table 5 — The least-square equations and regression coefficients for AZ_1solutions in DMSO at T = (298.15, 308.15, and 318.15) K.

Parameter	Least square equations (regression coefficients, R^2)		
	T = 298.15 K	T = 308.15 K	T = 318.15 K
ρ /(kg · m^{-3})	303.53 C + 1096.4 (0.990)	414.49 C + 1086 (0.992)	400.79 C + 1075.9 (0.994)
η / (mPa· s)	37.084 C + 1.864 (0.986)	17.209 C + 1.498 (0.993)	19.716 C + 1.291 (0.969)
U / (m · s^{-1})	805.48 C + 1499.2 (0.957)	847.12 C + 146.7 (0.978)	794.52 C + 1430 (0.988)
$Z \cdot 10^6$ /(kg · m^{-2} · s^{-1})	1.340 C + 1.643 (0.973)	1.529 C + 1.587 (0.986)	1.431 C + 1.539 (0.994)
$\kappa_s \cdot 10^{-10}$ /(Pa^{-1})	–5.433 C + 4.057 (0.966)	–6.570 C + 4.309 (0.983)	–6.625 C + 4.540 (0.992)
$L_f \cdot 10^{-11}$ /(m)	–2.833 C + 4.217 (0.967)	–3.326 C + 4.346 (0.983)	–3.286 C + 4.461 (0.992)
$R_m \cdot 10^{-4}$ /(m$^{10/3}$ · s$^{-1/3}$ ·mol^{-1})	–0.523 C + 8.154 (0.888)	–1.258 C + 8.162 (0.977)	–1.250 C + 8.180 (0.957)
$b \cdot 10^{-5}$ /(m^3)	–1.660 C + 7.025 (0.988)	–2.409 C + 7.091 (0.990)	–2.366 C + 7.154 (0.993)
$\pi \cdot 10^8$ /(Pa)	71.311 C + 7.653 (0.985)	37.937 C + 6.900 (0.992)	48.395 C + 6.649 (0.964)
$V_f \cdot 10^{-7}$ /(m^3)	–12.765 C + 0.556 (0.977)	–10.624 C + 0.749 (0.988)	–16.724 C + 0.904 (0.950)
$\tau \cdot 10^{-13}$ /(s)	184.35 C + 10.092 (0.985)	84.196 C + 8.611 (0.993)	106.04 C + 7.821 (0.959)
S_n	2E+09 C^4 - 4E+07 C^3 + 302112 C^2 - 449.3 C + 0.2309 (0.997)	3E+09 C^4 - 6E+07 C^3 + 405466 C^2 - 656.65 C + 0.3809 (0.997)	–5E+11 C^5 + 1E+10 C^4 – 2E+ 08 C^3 + 1E+06 C^2 – 4390.2 C + 3.2596 (1)

Table 6 — The least-square equations and regression coefficients for AZ_2solutions in DMSO at T = (298.15, 308.15, and 318.15) K.

Parameter	Least square equations (regression coefficients, R^2)		
	T = 298.15 K	T = 308.15 K	T = 318.15 K
ρ /(kg · m^{-3})	287.32 C + 1096.0 (0.978)	326.33 C + 1086.3 (0.988)	347.15 C + 1075.9 (0.985)
η / (mPa· s)	33.74 C + 1.863 (0.993)	16.233 C + 1.470 (0.994)	19.384 C + 1.292 (0.931)
U / (m · s^{-1})	908.49 C + 1499.2 (0.984)	826.3 C + 1462.7 (0.963)	760.55 C + 1431.4 (0.993)
$Z \cdot 10^6$ /(kg · m^{-2} · s^{-1})	1.429 C + 1.643 (0.990)	1.377 C + 1.588 (0.978)	1.318 C + 1.540 (0.992)
$\kappa_s \cdot 10^{-10}$ /(Pa^{-1})	–5.921 C + 4.0591 (0.988)	–6.094 C + 4.032 (0.972)	–6.221 C +4.536 (0.993)
$L_f \cdot 10^{-11}$ /(m)	–3.088 C + 4.218 (0.988)	–3.086 C + 4.343 (0.972)	–3.069 C + 4.459 (0.993)
$R_m \cdot 10^{-4}$ /(m$^{10/3}$ · s$^{-1/3}$ ·mol^{-1})	–0.257 C + 8.156 (0.871	–0.625 C + 8.162 (0.831)	–0.894 C + 8.182 (0.915)
$b \cdot 10^{-5}$ /(m^3)	–1.539 C + 7.028 (0.970)	–1.823 C + 7.089 (0.984)	–2.000 C + 7.154 (0.980)
$\pi \cdot 10^8$ /(Pa)	64.736 C + 7.648 (0.991)	35.767 C + 6.836 (0.993)	47.479 C + 6.648 (0.924)
$V_f \cdot 10^{-7}$ /(m^3)	–11.828 C + 0.558 (0.983)	–10.531 C + 0.770 (0.991)	–16.621 C+ 0.905 (0.901)
$\tau \cdot 10^{-13}$ /(s)	165.1 C + 10.09 (0.992)	79.807 C + 8.437 (0.994)	104.86 C + 7.818 (0.917)
S_n	9E+08C^4 - 2E+07C^3 + 166840C^2 – 141.1C + 0.0295 (0.993)	1E+09C^4 - 2E+07C^3 + 123910C^2 – 6.3647C - 0.0531 (0.99452)	–4E+12C^5 + 1E+11C^4 - 8E+08C^3 + 2E+06C^2 - 1779.8C + 0.0913 (1)

Table 7 — The least-square equations and regression coefficients for AZ_1 solutions in DMF at T = (298.15, 308.15, and 318.15) K.

Parameter	Least square equations (regression coefficients, R^2)		
	T = 298.15 K	T = 308.15 K	T = 318.15 K
ρ /(kg · m^{-3})	1090.6 C + 944.2 (0.999)	1067.1 C + 935.05 (0.980)	1034.9 C + 925.43 (0.987)
η / (mPa· s)	10.893 C + 0.821 (0.999)	8.680 C + 0.715 (0.989)	6.502 C + 0.621 (0.999)
U / (m · s^{-1})	892.6 C + 1456.7 (0.987)	743.29 C + 1418.1 (0.998)	786.08 C + 1380 (0.997)
$Z \cdot 10^6$ /(kg · m^{-2} · s^{-1})	2.442 C + 1.375 (0.999)	2.216 C + 1.326 (0.990)	2.164 C + 1.277 (0.995)
$\kappa_s \cdot 10^{-10}$ /(Pa^{-1})	–11.676 C + 4.990 (0.998)	–11.46 C + 5.317 (0.993)	–12.598 C + 5.673 (0.997)
$L_f \cdot 10^{-11}$ /(m)	–5.506 C + 4.677 (0.998)	–5.232 C + 4.828 (0.994)	–5.570 C + 4.987 (0.997)
$R_m \cdot 10^{-4}$ /(m$^{10/3}$ · s$^{-1/3}$ ·mol^{-1})	–7.876 C + 8.772 (0.999)	–8.019 C + 8.779 (0.970)	–7.692 C + 8.790 (0.978)
$b \cdot 10^{-5}$ /(m^3)	–8.331 C + 7.626 (0.999)	–8.315 C + 7.699 (0.978)	–8.215 C + 7.775 (0.986)
$\pi \cdot 10^8$ /(Pa)	34.491 C + 5.041 (0.999)	30.119 C + 4.734 (0.987)	25.335 C + 4.590 (0.990)
$V_f \cdot 10^{-7}$ /(m^3)	–26.60 C + 1.657 (0.997)	–29.525 C + 1.964 (0.981)	–30.16 C + 2.327 (0.998)
$\tau \cdot 10^{-13}$ /(s)	57.863 C + 5.471 (0.998)	49.238 C + 5.071 (0.986)	37.57 C + 4.704 (0.998)
S_n	4E+08C^4 - 1E+07C^3 + 169828C^2 – 634.95C + 1.5822 (0.990)	2E+09C^4 - 5E+07C^3 + 364653C^2 – 937.86C + 1.4999 (0.995)	4E+12C^5 - 1E+11C^4 + 1E+09C^3 – 6E+06C^2 + 12584C - 7.2445 (1)

Table 8 — The least-square equations and regression coefficients for AZ_2 solutions in DMF at T = (298.15, 308.15, and 318.15) K.

Parameter	Least square equations (regression coefficients, R^2)		
	T = 298.15 K	T = 308.15 K	T = 318.15 K
ρ /(kg · m^{-3})	1144 C + 953.36 (0.997)	1186 C + 942.87 (0.987)	1128.1 C + 933.24 (0.992)
η / (mPa· s)	11.025 C + 0.827 (0.997)	9.169 C + 0.7182 (0.983)	6.717 C + 0.623 (0.998)
U / (m · s^{-1})	811.4 C + 1457.1 (0.998)	793.95 C + 1418.4 (0.998)	800.41 C + 1380.4 (0.995)
$Z \cdot 10^6$ /(kg · m^{-2} · s^{-1})	2.450 C + 1.389 (0.998)	2.440 C + 1.337 (0.995)	2.313 C + 1.288 (0.994)
$\kappa_s \cdot 10^{-10}$ /(Pa^{-1})	–11.237 C + 4.939 (0.998)	–12.313 C + 5.271 (0.997)	–13.09 C + 5.622 (0.994)
$L_f \cdot 10^{-11}$ /(m)	–5.325 C + 4.653 (0.998)	–5.65 C + 4.807 (0.998)	–5.815 C + 4.964 (0.994)
$R_m \cdot 10^{-4}$ /(m$^{10/3}$ · s$^{-1/3}$ ·mol^{-1})	–8.328 C + 8.689 (0.997)	–8.826 C + 8.707 (0.979)	–8.356 C + 8.718 (0.988)
$b \cdot 10^{-5}$ /(m^3)	–8.574 C + 7.553 (0.997)	–9.096 C + 7.635 (0.986)	–8.813 C + 7.716 (0.991)
$\pi \cdot 10^8$ /(Pa)	35.287 C + 5.091 (0.999)	32.063 C + 4.771 (0.982)	26.458 C + 4.622 (0.999)
$V_f \cdot 10^{-7}$ /(m^3)	–26.557 C + 1.640 (0.998)	–30.655 C + 1.951 (0.972)	–30.856 C + 2.318 (0.997)
$\tau \cdot 10^{-13}$ /(s)	58.438 C + 5.454 (0.999)	51.075 C + 5.050 (0.974)	38.23C + 4.675 (0.997)
S_n	8E+08C^4 - 2E+07C^3 + 111054C^2 + 10.597C+ 0.0378 (0.99)	2E+09C^4 - 3E+07C^3 + 175744C^2 – 26.367C + 0.0101 (0.979)	y = –1E+11C^5 + 2E+09C^4 + 1E+07C^3 – 362214C^2 + 2004.6C - 1.4728 (1)

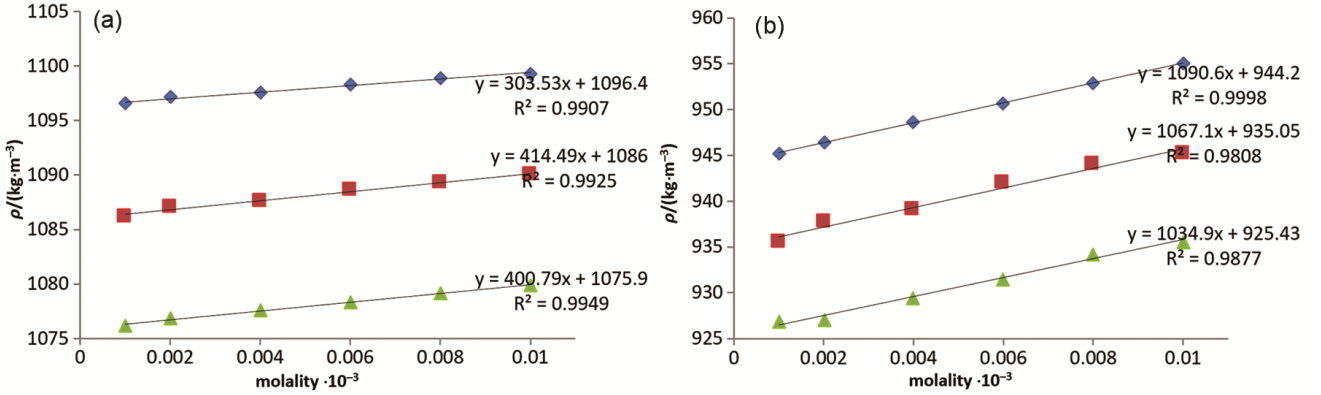

Fig. 2 — The plots of Density (ρ) against molality (m) for AZ_1 in (a) DMSO at 298.15K (♦), 308.15K (■) and 318.15K (▲); (b) DMF at 298.15K (♦), 308.15K (■) and 318.15K (▲).

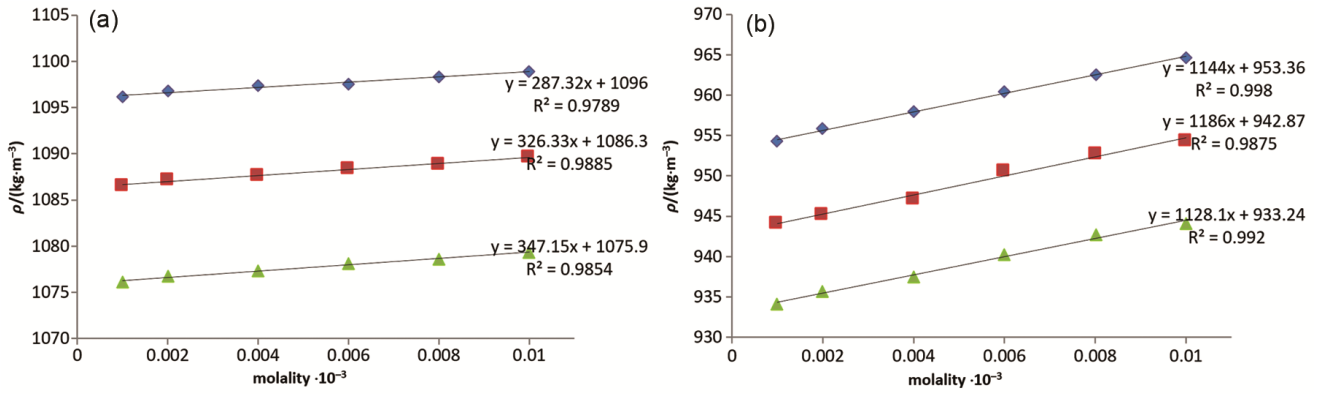

Fig. 3 — The plots of Density (ρ) against molality (m) for AZ_2 in (a) DMSO at 298.15K (♦), 308.15K (■) and 318.15K (▲); (b) DMF at 298.15K (♦), 308.15K (■) and 318.15K (▲).

ultrasonic velocity (U) and concentration (C) (R^2 = 0.957–0.998). A good to outstanding linear relationship between the factors under investigation is shown by all of these correlations. The rise in density (ρ), viscosity (η), and ultrasonic velocity (U) with concentration (C) indicates that there were likely large molecular interactions that caused the cohesive forces to expand; on the other hand, the reduction in the same parameters with temperature (T) implies that cohesive forces contracted. The rise in density, viscosity, and ultrasonic velocity with concentration indicates that cohesive forces have expanded due to

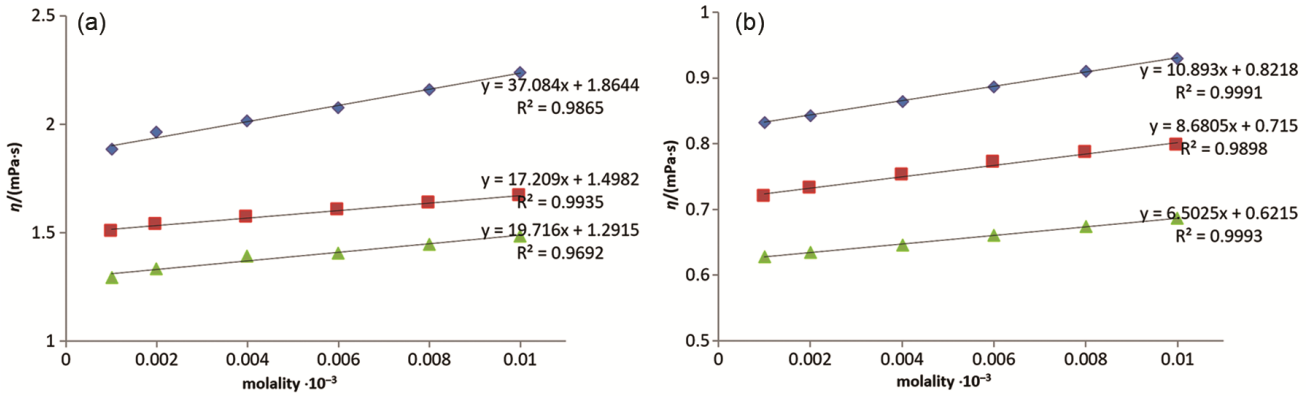

Fig. 4 — The plots of Viscosity (η) against molality (m) for AZ_1 in (a) DMSO at 298.15K (♦), 308.15K (■) and 318.15K (▲); (b) DMF at 298.15K (♦), 308.15K (■) and 318.15K (▲).

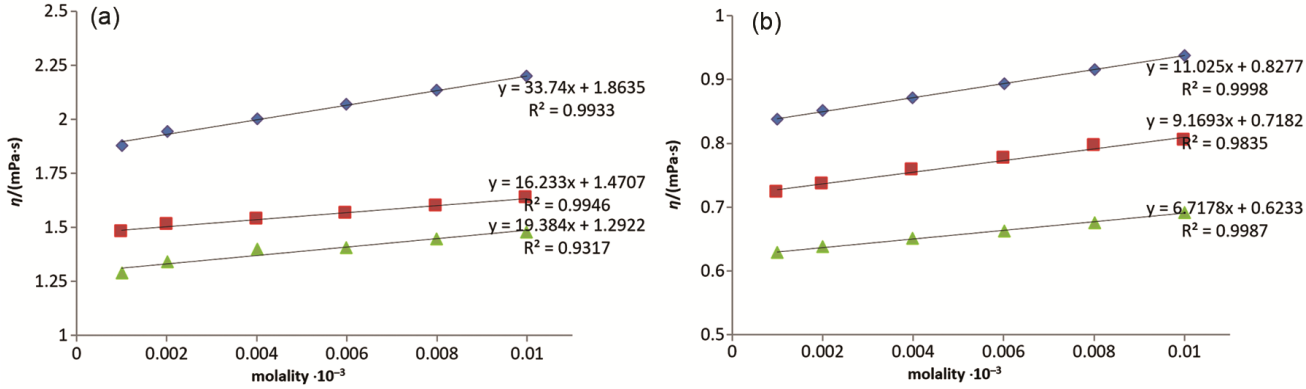

Fig. 5 — The plots of Viscosity (η) against molality (m) for AZ_2 in (a) DMSO at 298.15K (♦), 308.15K (■) and 318.15K (▲); (b) DMF at 298.15K (♦), 308.15K (■) and 318.15K (▲).

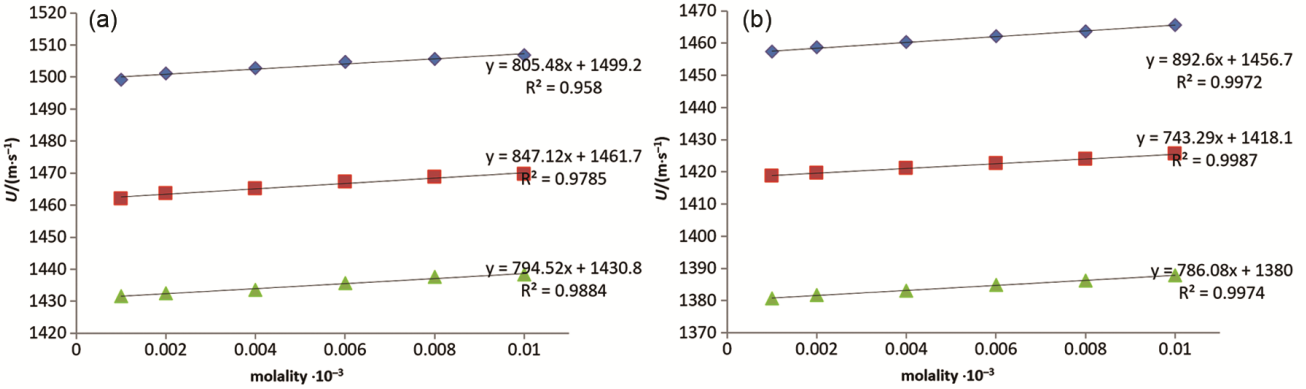

Fig. 6 — The plots of Ultrasonic sound velocity (U) against molality (m) for AZ_1 in (a) DMSO at 298.15K (♦), 308.15K (■) and 318.15K (▲); (b) DMF at 298.15K (♦), 308.15K (■) and 318.15K (▲).

strong molecular connections; the reduction in these same parameters with temperature (T) indicates that cohesive forces have constricted. The density, viscosity, pressure, temperature, and other properties of the medium all impact velocity. Due to significant molecular connections, cohesive forces have extended as indicated by the rise in density, viscosity, and ultrasonic velocity with concentration; on the other hand, cohesive forces have constricted as indicated by the decrease in these same parameters with

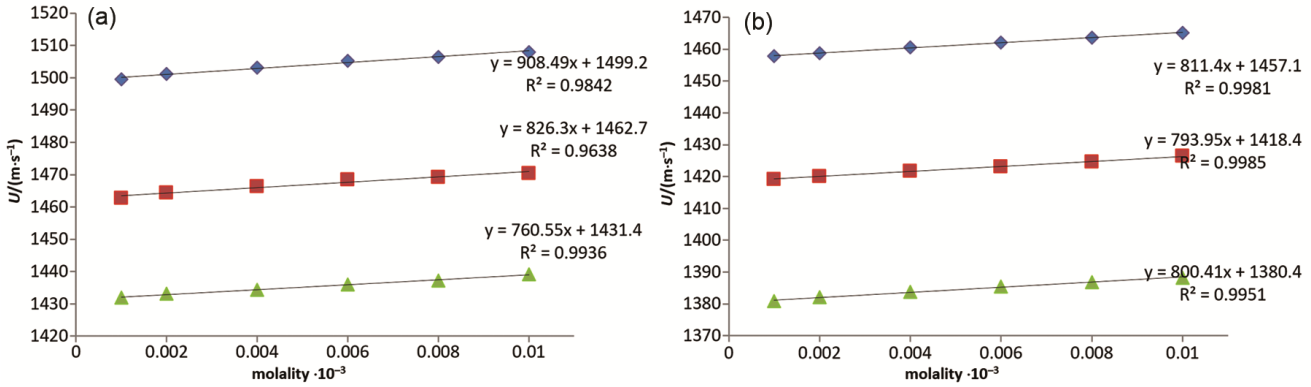

Fig. 7 — The plots of Ultrasonic sound velocity (U) against molality (m) for AZ_2 in (a) DMSO at 298.15K (♦), 308.15K (■) and 318.15K (▲); (b) DMF at 298.15K (♦), 308.15K (■) and 318.15K (▲).

Table 9 — Variation of Gibbs free energy of activation, ΔG*, enthalpy of activation,ΔH*and entropy of activation,ΔS*with concentration for AZ_1 in different solvent systems at T = (298.15, 308.15, and 318.15) K.

System	$\Delta G^*/$ (J ·mol^{-1})			ΔH^*/(kJ ·mol^{-1})	ΔS^* /(J · K^{-1}·mol^{-1})
	T = 298.15 K	T = 308.15 K	T = 318.15 K		
DMSO+ AZ_1	4614.0	4389.5	4508.6	6.26	5.70
	4708.3	4434.2	4573.5	6.78	7.17
	4774.1	4480.6	4685.2	6.16	4.92
	4830.5	4522.3	4706.7	6.76	6.72
	4932.3	4566.8	4770.6	7.42	8.66
	5010.2	4613.8	4828.0	7.83	9.79
DMF+ AZ_1	3101.7	3034.0	2986.5	4.88	5.98
	3125.8	3067.9	3010.6	4.82	5.69
	3173.8	3124.8	3046.8	5.09	6.42
	3225.8	3175.3	3093.3	5.19	6.58
	3281.9	3217.3	3127.7	5.58	7.72
	3320.1	3244.6	3170.6	5.54	7.46

temperature (T). The density, viscosity, pressure, temperature, and other properties of the medium all impact velocity. The concentration and temperature dependence of acoustical parameters allows for a detailed determination of the molecular interaction strength in the solutions of AZ_1 and AZ_2.

There is an inverse relationship between ultrasonic velocity (U) and intermolecular free path length (L_f). As can be shown in Tables 5, 6, 7, and 8, solute velocity (V) and acoustical impendence (Z) increased with concentration (C) and decreased with temperature (T) in DMSO and DMF systems. Solvent-solute interactions led to a considerable alteration in a structural arrangement for both derivatives. Intermolecular free path length (L_f) was seen to grow with T for both derivatives and decrease with concentration, as demonstrated in Tables 5, 6, 7, and 8, suggesting the existence of solvent-solute interactions. The Ultrasonic velocity (U) distribution of the system gives information on the average length of the relaxation process that generated the distribution.

The observed viscous relaxation time (τ) was caused by the structural relaxation processes. Multiple molecules move in unison around a hole in the system, which causes the molecules to rearrange themselves. It was found that the viscosity relaxation time (τ) of the two mixes decreased with temperature (T) and increased with concentration (C) in both binary systems (Tables 5–8).

The equation was used to calculate the value of ΔG^* at different concentrations and temperatures, and it was compared to an infinite dilution (R2 = 0.955-0.999). An overview of how the AT_1 and $AT_2\Delta G^*$ values vary with C and T can be seen in Table 9 and Table 10. The least squares intrinsic values of ΔG^* for AZ_1 in DMSO systems were found to be linearly raised with C and linearly reduced (for 308.15 K) with T, in contrast to DMF systems where ΔG^* was found to linearly rise with C and linearly fall with T (Fig. 8). The –F group located at position 4 in the structure of solute AZ_1 may be the reason for its behavior (Fig. 1). Fig. 9 shows that whereas ΔG^*

Table 10 — Variation of Gibbs free energy of activation, ΔG*, enthalpy of activation,ΔH*and entropy of activation,ΔS*with concentration for AZ_2 in different solvent systems at T = (298.15, 308.15, and 318.15) K.

System	ΔG^*/ (J ·mol^{-1})			ΔH^*/(kJ ·mol^{-1})	ΔS^* /(J · K^{-1}·mol^{-1})
	T = 298.15K	T = 308.15K	T = 318.15K		
DMSO+ AZ_2	4612.0	4340.3	4292.2	9.41	16.22
	4686.0	4381.9	4398.4	9.02	14.71
	4755.8	4423.0	4503.2	8.59	13.06
	4824.3	4461.0	4513.7	9.52	15.97
	4895.1	4509.3	4574.2	9.75	16.53
	4963.1	4557.8	4629.2	10.02	17.20
DMF+ AZ_2	3092.9	3020.9	2969.0	4.94	6.20
	3120.4	3057.2	2996.5	4.96	6.18
	3168.2	3123.4	3037.7	5.10	6.47
	3220.1	3169.7	3074.9	5.37	7.20
	3272.2	3220.0	3113.2	5.63	7.88
	3318.1	3237.4	3161.5	5.65	7.82

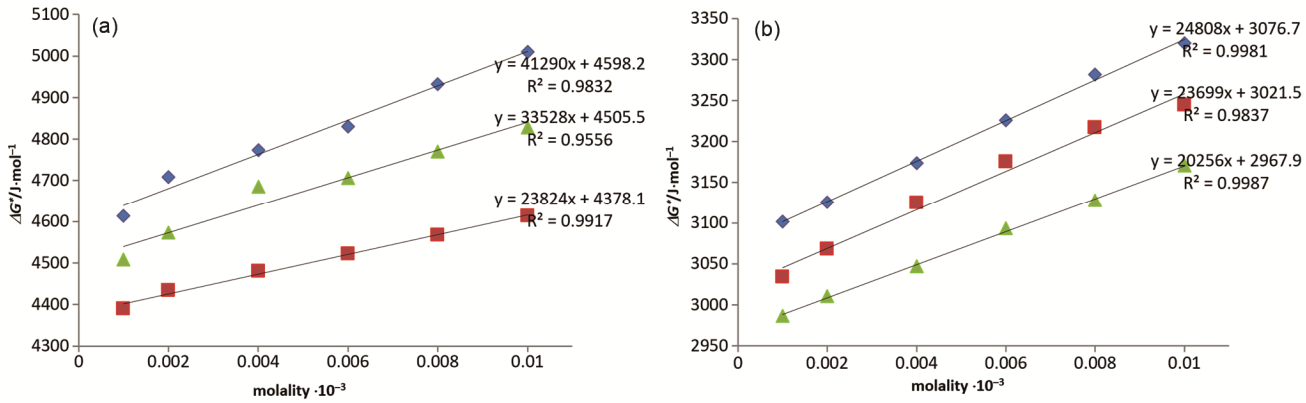

Fig. 8 — The plots of Gibbs free energy of activation (*ΔG**) against molality (*m*) for AZ_1 in (a) DMSO at 298.15K (♦), 308.15K (■) and 318.15K (▲); (b) DMF at 298.15K (♦), 308.15K (■) and 318.15K (▲).

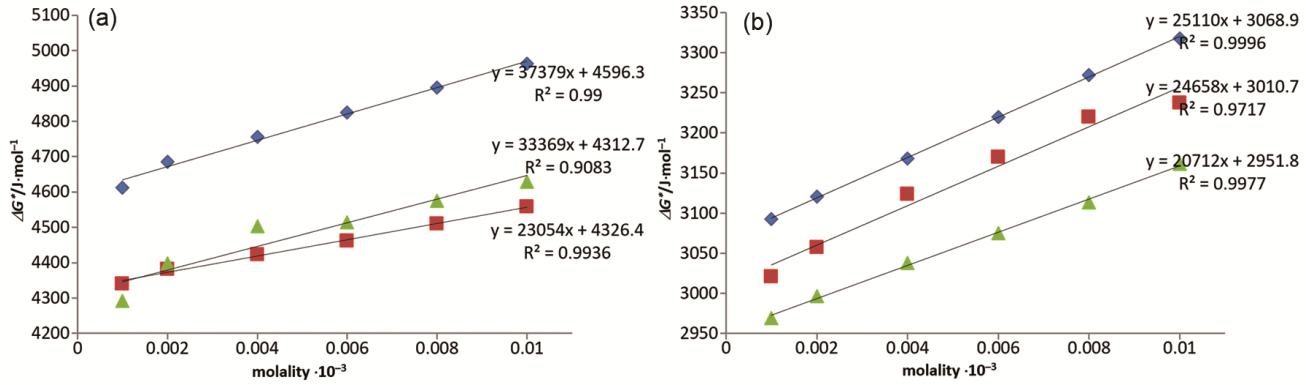

Fig. 9 — The plots of Gibbs free energy of activation (*ΔG**) against molality (*m*) for AZ_2 in (a) DMSO at 298.15K (♦), 308.15K (■) and 318.15K (▲); (b) DMF at 298.15K (♦), 308.15K (■) and 318.15K (▲).

decreased linearly with *C* and increased linearly with *T* in DMF solutions, *ΔG** for AZ_2 intrinsic least squares values grew linearly with *C* and *T* in DMSO systems, with the exception of 318.15 K. The reason for the behavior of solute AZ_2 may be attributed to the presence of $–CH_3$ at position 4 in its structure, which sets it apart from AZ_1 (see Fig. 1). The *ΔG** values for AZ_1 and AZ_2 in both solvent systems were positive, suggesting that there had been molecular interaction in the mixtures. The distinct physical properties of the solute, such as concentration in the phase and absorption due to molecular rearrangement, were also

demonstrated to be independent of *C* by the linear difference between *ΔG**and *C*. The activation enthalpy (*ΔH**) and entropy (*ΔS**) findings from DMSO and DMF solutions at T = (298.15, 308.15, and 318.15 K) are briefly summarized in Table 9 and Table 10. The *ΔH** values for AZ_1 and AZ_2 in both binary systems were positive at all experimental temperatures. The positive values of *ΔH** indicate that the process was endothermic. At every experimental temperature, the values of *ΔS** for AZ_1 and AZ_2 in the DMSO and DMF systems were positive. Given the positive value of *ΔS**, the complex's growth was most likely the result of spontaneous activity. The values of *ΔS** and *ΔH** for AZ_1 and AZ_2 in DMSO and DMF solutions were positive at all temperatures, suggesting that the reaction was not spontaneous and that the transition state was connected to the formation of bonds. The structure of compound AZ_1 was found to be more labile in its lattice, whereas the structure of compound AZ_1 was determined to have been more compact in its lattice based on the analytical results. This was made clear by the results shown in Table 9 and Table 10, where it was discovered that *ΔS** in AZ_2, which exhibits higher flexibility in complex formation and solute-solvent interaction, differed widely.

The reduction in isentropic compressibility (κ_S) might be attributed to the aggregation of solvent molecules around solute molecules, which fosters strong solvent-solute interactions. Furthermore, it was demonstrated that in both binary combinations, mixtures AZ_1 and AZ_2's isentropic compressibility (κ_S) rose with *T* and fell with *C*. The fully compressed solvated molecules brought on by the electrical forces of the ion are responsible for this occurrence. The compressibility of the solution was largely caused by the unbound solvent molecules. The compressibility of the solution diminishes as the solute concentration increases because of interactions between the solute and the solvent in the system. This was further corroborated by the increase in viscosity for AZ_1 and AZ_2 solutions in DMSO and DMF systems. The results revealed that DMF had the highest isentropic compressibility (κ_S), which led to the discovery of this.

AZ_1 and AZ_2 have not produced any complexes or aggregates in the DMSO and DMF systems, based on the linear fluctuations in the Rao's molar sound function (*Rm*) and Van der Waals constant (*b*) (correlation coefficient R^2 = 0.831-0.999) shown in Tables 5, 6, 7, and 8. The forces of attraction and repulsion among the organisms in the solution generate the internal pressure (π). For AZ_1 and AZ_2, *C,* and *T* both increased and lowered the values of intermolecular free path length and isentropic compressibility(κ_S). Based on the internal pressure (π) results, which showed that it was extended, this was decided. With the exception of AZ_1 at *T* = 318.15K in DMSO, the internal pressure of the two derivatives in both binary systems rose with *C* and fell with *T*. The varying internal pressure performance of pyrimidine-substituted thiazolidinone derivatives was also caused by the distinct solute molecule orientations in DMSO and DMF solutions. The free volume (V_f) of a solute molecule at a specific temperature and pressure is determined by the internal pressure of the liquid in which it was dissolved. An improvement in cohesive forces is specified in the solutions of AZ_1 and AZ_2 in both binary systems by a decrease in free volume (V_f) and an increase in internal pressure (π), and *vice versa*. The system's expansion in internal pressure and reduction in free volume with concentration both point to an ordered structural arrangement because of the system's lowering entropy. Tables 5, 6, 7, and 8 demonstrated that the internal pressure rose and the free volume dropped for AZ_1 and AZ_2 in both binary systems. This confirmed once more that interactions between solutes and solvents exist in the binary system that has been studied up to this point.

Solvation number (S_n) relationships were also employed to measure the degree of interaction. The interactions between the solute and the solvent determine how important the S_n is. It is clear from Tables 5, 6, 7, and 8 that solvation affected the DMF system more than the DMSO system. The findings unequivocally demonstrate that the Sn values were optimistic, indicating that the tendency to form structures was present in both binary systems' AZ_1 and AZ_2. Based on the difference in S_n with *C* and *T* values, strong dipole-dipole interactions could have happened.

Conclusions

The objective of the current investigation was to ascertain the significance of the solution study. The solute-solvent and solute-solute interactions were calculated at three different temperatures (298.15, 308.15, and 318.15 K) using these variables. On the basis of their structural similarities, the

behaviors of compounds AZ_1 and AZ_2 in DMSO and DMF were connected. Due to the electron-withdrawing nature of the character of the –F group in AZ_1 and the electron-donating nature of the $–CH_3$ group in AZ_2, different behaviors of both derivatives in DMSO and DMF were occasionally observed. This came about as a result of the significant roles that both groups interacted with molecules. There has been contact between the molecules in the mixture when the Gibbs free energy of activation is positive. The structure formed as a judgment on the basis of positive values of solvation number due to significant molecular interactions. The density (ρ), viscosity (η), and ultrasonic velocity (U) all rose as T and C increased, according to the experimental data. The many thermodynamic characteristics investigated in this paper suggest the presence of strong and weak dispersive forces in binary mixtures. This work further demonstrates that the binary systems under consideration use pyrimidine-substituted thiazolidinone derivatives as a structural former.

Supplementary Information

Supplementary information is available in the website http://nopr.niscpr.res.in/handle/123456789/58776.

Acknowledgment

The authors are thankful to the Department of Chemistry and Maharaja Krishnakumarsinhji Bhavnagar University for providing the necessary facilities to carry out this work.

References

1 Genchi G G, Marino A, Tapeinos C & Ciofani G, *Front bioeng biotech,* 18 (2017) 80.
2 Zhou W, Sarpong F & Zhou C, *Foods,* 11 (2022) 2874.
3 Mardanshahi A, Nasir V, Kazemirad S & Shokrieh M M, *Comp Struc,* 246 (2020) 112403.
4 Bandral A & Kumar A, *J MolLiq*, 348 (2022) 118081.
5 Sharma T, Bandral A, Bamezai R K & Kumar A, *J Chem Therm*, 6 (2022) 100043.
6 Pandiselvam R, Aydar A Y, Kutlu N, Aslam R, Sahni P, Mitharwal S, Gavahian M, Kumar M, Raposo A, Yoo S & Han H, *Ultra Sonochem,* 7 (2022) 106261.
7 Abbas F H, Naife T M, Ahmed D J & Hasan E B, *J Pet,* 13 (2023) 86.
8 Dubey G P &Dhingra L, *Int J Thermophys,* 3 (2022) 30.
9 Dange S P, Chimankar O P & Borkar P D, *IJPAP*, 59 (2021) 132.
10 Gaba R, Kaur N, Pal A & Sharma D, *J Mol Liq,* 380 (2023) 121766.
11 Xu L, Xue F, Zheng H, Ji Q, Qiu C, Chen Z, Zhao X, Li P, Hu Y, Peng Q & He X, *Nano Ene,* 103 (2022) 107848.
12 Foroughi F, Lamb J J, Burheim O S &Pollet B G, *Catal,* 11 (2021) 284.
13 Sharma T, Bandral A, Bamezai R K & Kumar A, *J Chem Thermodyn,* 6 (2022) 100043.
14 Sachdeva H, Khaturia S, Saquib M, Khatik N, Khandelwal A R, Meena R & Sharma K, *Appl Biochem Biotech*, 194 (2022) 6438.
15 Singh P, Rathi P, Singhal S & Rajput C, *Int J Pharm Res,* 14 (2022) 09752366.
16 Elkanzi N A, Hrichi H, Alolayan R A, Derafa W, Zahou F M & Bakr R B, *ACS Omega,* 7 (2022) 27769.
17 Godhani D R, Dobariya P B, Sanghani A M, Jogel A A & Mehta J P, *J Mol Liq,* 180 (2013) 179.
18 Shekaari H, Bezaatpour A & Soltanpour A, *J Chem Amp Eng,* 55 (2010) 5927.
19 Gokavi G S, Raju J R, Aminabhavi T M, Balundgi R H & Muddapur M V, *C J ChemEng Data*,1 (1986) 15.
20 Keshapolla D &Gardas R L, *Fluid Phase Equ*, 383 (2014) 32.
21 Nagarjun B, Sarma A V, Rao G V &Rambabu C, *J Therm,* 10 (2013) 285796.
22 Chauhan S, *IJPAP,* 51 (2016) 531.
23 Thakre N, Prajapati A K, Mahapatra S P, Kumar A, Khapre A & Pal D, *J Chem Amp Eng,* 61 (2016) 2614.
24 Baluja S & Shah A, *Fluid Phase Equilib*, 215 (2004) 55.
25 Hirai N &Eyring H, *J Appl Phys,* 29 (1958) 810.